Extended Data Figures

for

Sequence-specific interactions determine viscoelastic moduli and aging dynamics of protein condensates

Authors: Ibraheem Alshareedah[1,§], Wade M. Borcherds[2,§], Samuel R. Cohen[3,4,§], Mina Farag[3], Anurag Singh[1], Anne Bremer[2], Rohit V. Pappu[3,*], Tanja Mittag[2,*], Priya R. Banerjee[1,*]

Affiliations:

[1]Department of Physics, The State University of New York at Buffalo, Buffalo, NY 14260, USA

[2]Department of Structural Biology, St. Jude Children's Research Hospital, Memphis, TN 38105, USA

[3]Department of Biomedical Engineering and Center for Biomolecular Condensates, Washington University in St. Louis, St. Louis, MO 63130, USA

[4]Center of Regenerative Medicine, Washington University in St. Louis, St. Louis, MO 63130, USA

§Equal contributions

*Corresponding authors. pappu@wustl.edu; tanja.mittag@stjude.org; prbanerj@buffalo.edu

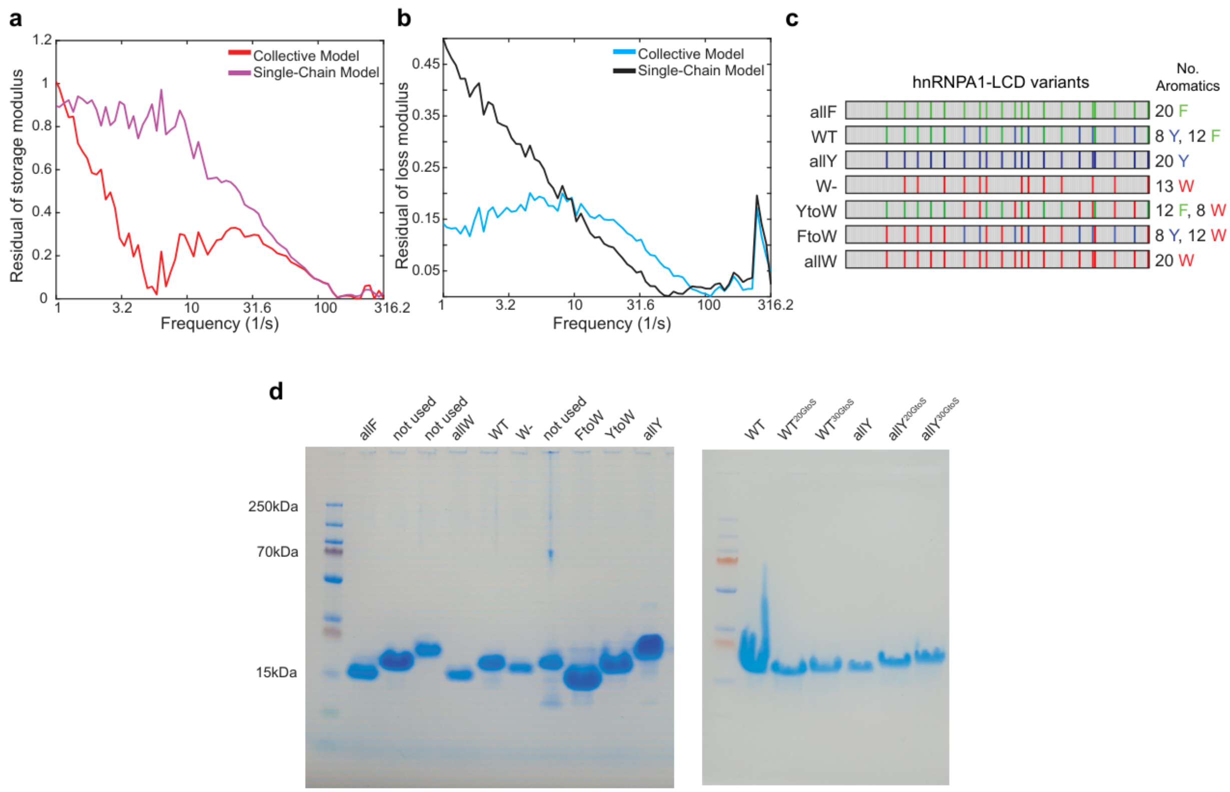

ED Fig. 1. (a) Residuals for condensates formed by WT A1 LCD between computed storage modulus using the single-chain (magenta) and collective models (red) referenced to the measured storage modulus. The residuals were computed as the absolute values of differences between the logarithms of the computed and measured moduli. Values of zero imply exact matches, values of one imply a discrepancy of an order of magnitude, and so on. At low frequencies, the sharp increase in residuals for the collective model is partly due to increased noise in the experimentally derived storage moduli. **(b)** Residuals between computed loss modulus using the single-chain (black) or collective chain dynamics (blue) and measured loss modulus for WT. The residuals were computed as in panel (**a**). **(c)** A schematic diagram of the constructs deployed in the various measurements summarized in this work. Grey represents non-aromatic spacer residues, whereas colored stripes represent the locations of the indicated aromatic residues. (**d**) SDS-PAGE gel image of purified proteins used for the experiments.

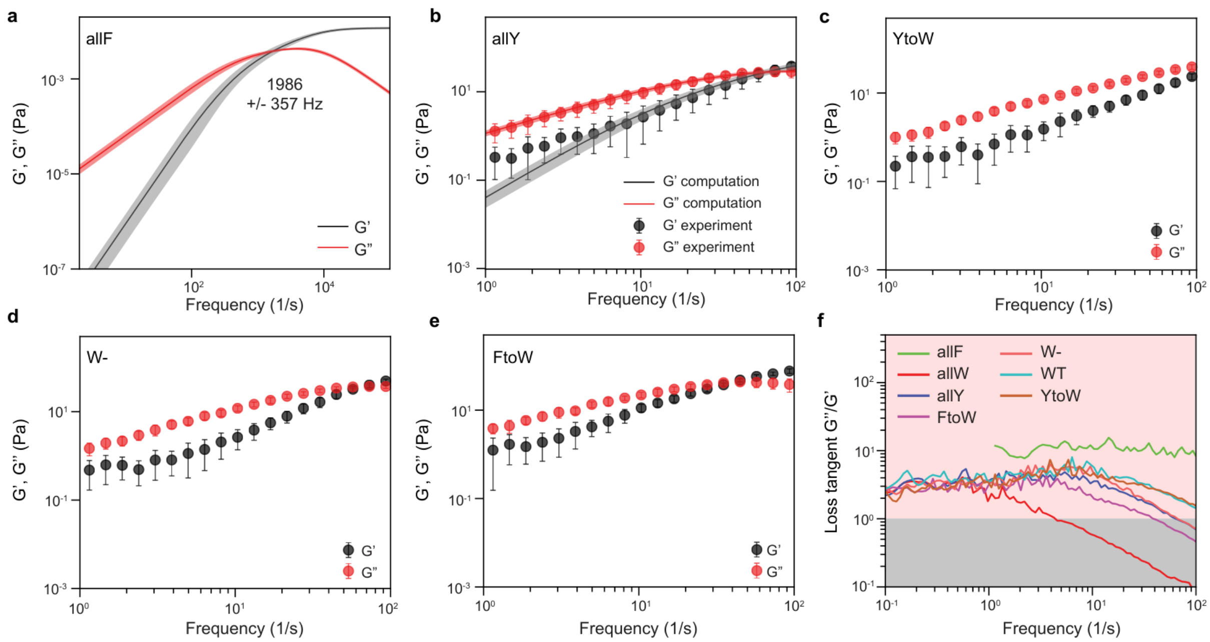

ED Fig. 2. (a) Computed dynamical moduli for condensates formed by allF. Analysis of the simulation results was performed using the collective model. This variant, as with all other variants, forms nascent condensates that are Maxwell fluids. The crossover frequency is indicated in the legend. The error band for the computed data represents the standard deviation from 3 replicates. **(b)** Measured dynamical moduli (symbols) for condensates formed by allY. Error bars represent the standard deviation as calculated from the moduli of 20 condensates. Also plotted are the computed moduli based on the analysis of simulation results using the collective model (lines). Error bands are calculated as in (**a**). **(c)-(e)** Measured dynamical moduli for condensates formed by **(c)** YtoW, **(g)** W-, and **(e)** FtoW variants of A1 LCD. Error bars are standard deviations as calculated from the moduli of 20 condensates. **(f)** Loss tangents for different variants and plotted against frequency. The loss tangents are calculated from measured moduli. The shaded regions are color coded as follows: *red* indicates dominantly viscous behavior; *grey* indicates dominantly elastic behavior.

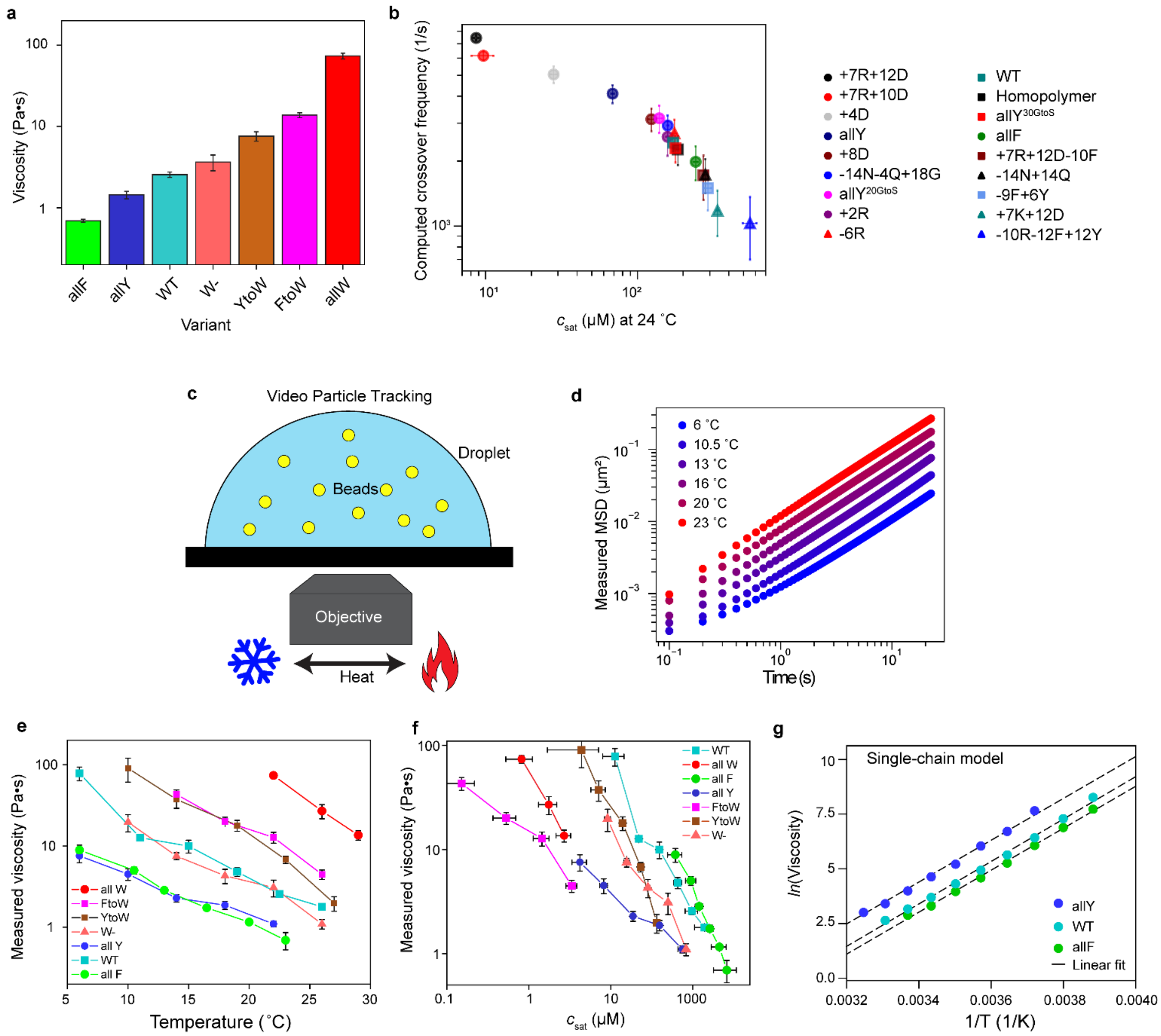

ED Fig. 3. (a) Room-temperature viscosity of condensates formed by different sequence variants of A1 LCD as measured by video particle tracking. Data is collected from at least five trials featuring at least ~50 tracked particles per trial. Error bars represent ±1 standard deviation. **(b)** Computed crossover frequencies were calculated by analyzing simulation results using the collective model. The results are plotted against the c_{sat} values computed at room temperature. The crossover frequency is the inverse of the network reconfiguration time of the respective condensate. **(c)** Schematic for the temperature-dependent video particle tracking experiment. Diffusion of multiple 200 nm polystyrene beads is recorded at distinct temperatures. **(d)** Representative plots of the ensemble-averaged MSD of 200 nm polystyrene beads within condensates formed by allF. Measurements were made using video particle tracking microrheology at different temperatures as set by a custom-made thermal stage attached to the microscope. **(e)** Measured temperature-dependent viscosities for the condensates formed by different sequence variants of A1 LCD used for the Arrhenius plots in Fig. 2c. **(f)** Measured temperature-dependent viscosities for condensates formed by different variants plotted against the temperature-dependent c_{sat} values. **(g)** Arrhenius plots for viscosities calculated from analysis of simulation results using the single-chain model.

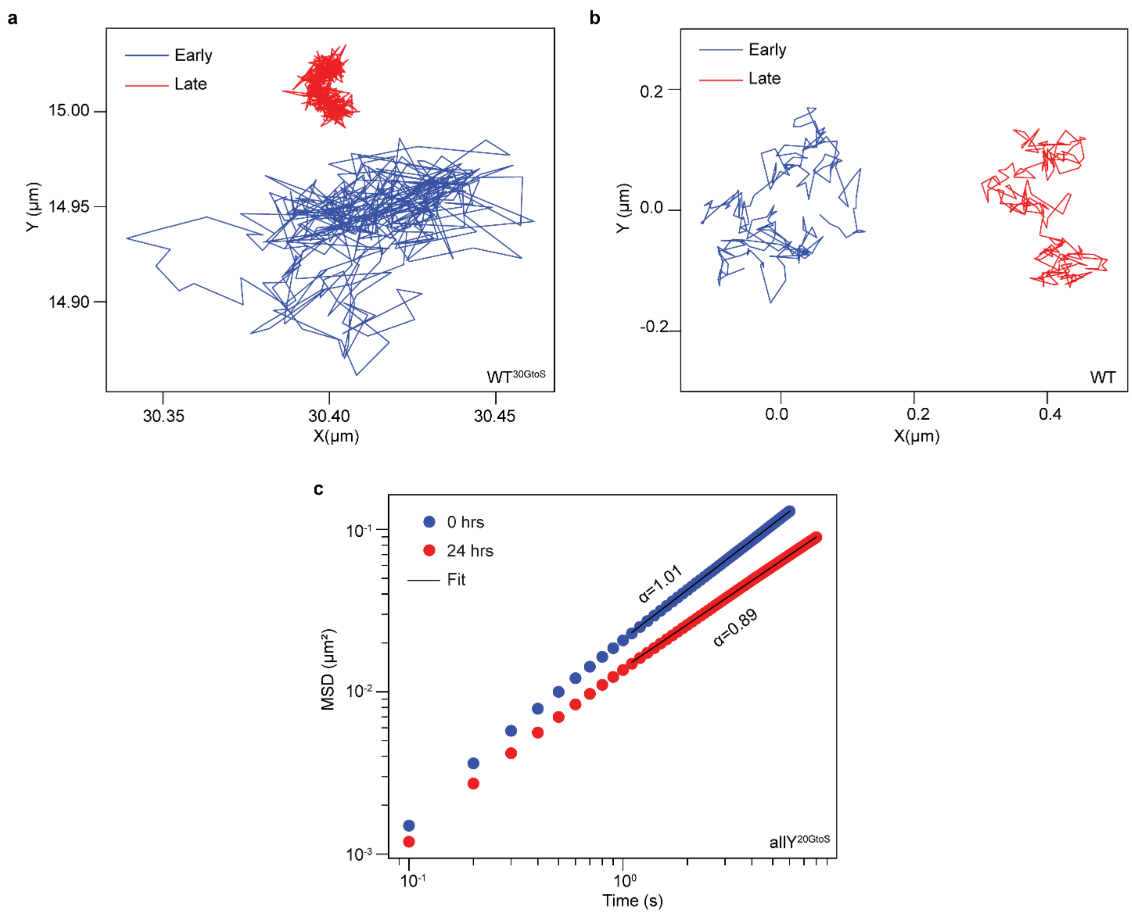

ED Fig. 4. (a) Trajectory of a 200 nm bead within freshly prepared condensate of WT^{30GtoS} variant of A1 LCD (blue) and approximately 2 minutes after the start of imaging (red). These data show that WT^{30GtoS} condensates undergo dynamical arrest within a short timescale. **(b)** Same as **(a)** but for WT A1 LCD condensate. **(c)** Ensemble-averaged MSD of 200 nm beads in fresh (0 hrs) or aged (24 hrs) condensates formed by allY^{20GtoS}. Solid lines are the fits to the equation $MSD(\tau) = 4D\tau^{\alpha} + N$. Also indicated are the values of the diffusivity exponent obtained from the fits, which show a clear deviation from the linear behavior for the aged condensates, indicating sub-diffusive motion of the probe particles.

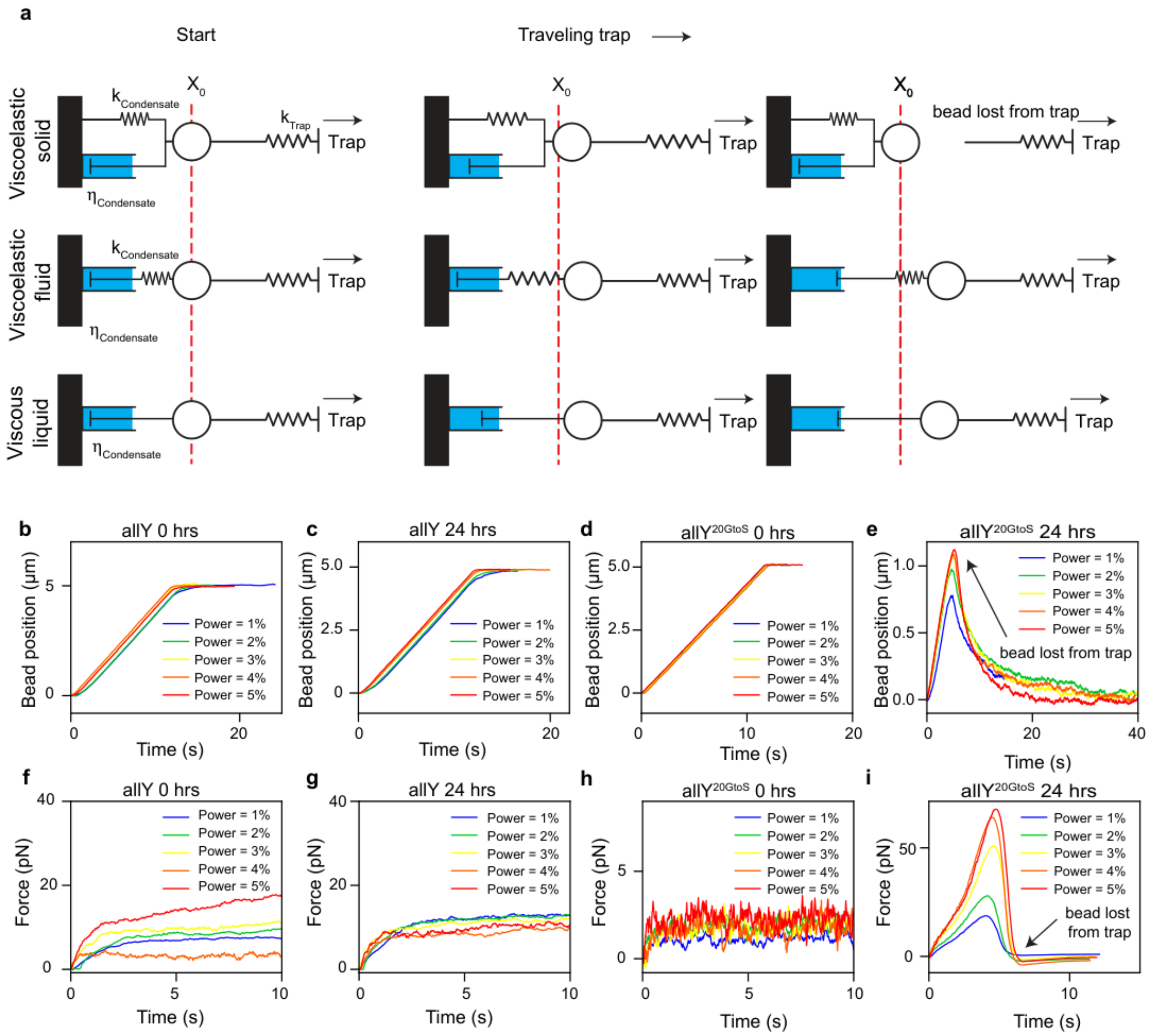

ED Fig. 5. (a) A schematic showing the expected outcomes of a particle embedded within a viscoelastic Kelvin-Voigt solid (top), viscoelastic Maxwell fluid (middle), and viscous liquid (bottom) upon creep deformation by an optical trap. As the optical trap exerts a force to drag a particle embedded within the fluid medium, the dashpot element applies a dissipative drag force while the spring element applies a restoring force. Except for the viscoelastic solid, the creep deformation is irreversible (the final bead position is distinct from the initial bead position X_0, indicated by the red vertical line). In the case of a viscoelastic solid, the bead recoils back to its initial position due to the stored energy within the elastic spring. In both viscoelastic fluids and viscous liquids, the deformation energy is eventually dissipated through the dashpot or the viscous element, giving rise to a terminally viscous behavior. **(b)** Bead position as a function of time in response to the programmed trap movement in nascent allY condensates at increasing power levels of the trapping laser. **(c)** Same as (**b**) but for the allY condensates after 24 hours following sample preparation. **(d)** Bead position as a function of time in response to the programmed trap movement in nascent allY^{20GtoS} condensates at increasing power levels of the trapping laser. **(e)** Same as (**d**) but for the allY^{20GtoS} condensates after 24 hours. **(f)** The force exerted on the bead by the allY condensate network in (**b**). **(g)** The force exerted on the bead by the allY condensate network in (**c**). **(h)** The force exerted on the bead by the allY^{20GtoS} condensate network in (**d**). **(i)** The force exerted on the bead by the allY^{20GtoS} condensate network in (**e**).